The Impact of Geometric and Surface Electronic Properties of Pt-Catalysts on the Particle Size Effect in Electrocatalysis

K. J. J. Mayrhofer,* B. B Blizanac, M. Arenz,† V. R. Stamenkovic, P. N. Ross, and N. M. Markovic

Materials Science Division, Lawrence Berkeley National Laboratory, University of California, Berkeley, California 94720

Received: April 5, 2005; In Final Form: May 10, 2005

The particle size effect on the formation of OH adlayer, the CO bulk oxidation, and the oxygen reduction reaction (ORR) have been studied on Pt nanoparticles in perchloric acid electrolyte. From measurements of the CO displacement charge at controlled potential, the corresponding surface charge density versus potential curves yielded the potentials of total zero charge (pztc), which shifts approximately 35 mV negative by decreasing the particle size from 30 nm down to 1 nm. As a consequence, the energy of adsorption of OH is more enhanced, that is, at the same potential the surface coverage with OH increases by decreasing the particle size, which in turn affects the catalytic reactions thereon. The impact of the electronically induced potential shift in the OH adsorption is demonstrated at the CO bulk oxidation, in which adsorbed OH is an educt species and promotes the reaction, and the ORR, where it can act as a surface site blocking species and inhibits the reaction.

1. Introduction

Decades before the prefix "nano" appeared so prominently in the scientific lexicon, catalytic chemists had already realized that unique catalytic properties were obtained on metallic clusters in the diameter range of 1−10 nm, for example, refs 1−4. In the scale of this dimension, two kinds of parameters can control the catalytic activity of nanoparticles: electronic factors, mainly related to the surface electronic structure and energetics,[5] and geometric factors, naturally believed to be associated with the topography of atom distribution on the catalysts' surface.[6] The two parameters, however, are only nominally separated,[7] since in metals the surface atomic structure influences the formation of a surface dipole moment (described here by the surface potential χ^{M}), which in addition to the chemical potential of electrons in the metal ($\mu_e{}^{M}$) contributes to the value of the work function Φ^{M}: $\Phi^{M}N_A = \mu_e{}^{M} + F\chi^{M}$[8,9] ($N_A$ is the Avogadro constant). Given that the distribution of surface atoms varies with the characteristic dimension of the aggregates, each size cluster may exhibit unique electronic and structural properties. This would generate what is now widely known in heterogeneous catalysis as the "crystallite size effect", that is, the variation of the reaction rate or selectivity with the characteristic dimension of a metallic catalyst.

The effect of Pt crystallite size on the kinetics of the oxygen reduction reaction (ORR) is a long-standing problem in electrocatalysis. An excellent review of the experimental work on carbon-supported Pt prior to about 1990 was presented by Kinoshita.[10] He came to the conclusion that the observed particle size effect in the case of the ORR can be attributed to the structural sensitivity, that is, the dependence on the geometry of the surface. For cubooctahedral particles, which consist of (111) and (100) facets bounded by low coordination number (edge and corner) atoms, simple geometric considerations indicate that the relative concentration of surface atoms on facets or in edge and corner positions changes dramatically as the crystallite size decreases in the 10−1 nm particle regime. For instance, if low coordination sites are especially active (or inactive) for a certain process, then one should also see a tremendous variation in catalytic activity (per unit surface atom or turnover number) in the nanoparticle regime. Although this approach did provide some new insight into the relationship between the structure sensitivity and the particle size effect, in many cases this purely geometric tactic has also shown significant weaknesses. The most profound one is probably that the (111) facet is the most active for the ORR in KOH but the least active in sulfuric acid, opposite to what thus would be expected; however, the same decreasing trend for the specific activity with the particle size can be seen in both electrolytes.[11] A completely different explanation for this effect was proposed by Watanabe et al.[12] In his territory theory, he claims that a mutual influence on the diffusion, "or some other parameters", exists when Pt-particles are close together, so that not all of the Pt surface area is usable for the reaction. The particle size effect is thereafter not truly dependent on the crystallite size but rather on the interparticle distances, with a critical distance of 20 nm above which the specific activity was constant. This hypothesis was disproved by Giordano et al.,[13] who found no evidence that the interparticle distance on the electrocatalytic activity play any role in the observed variations of the ORR with particle dimensions. More recently, Takasu et al.[14] have attributed the origin of particle size effects in the ORR to stronger interaction of oxygen with smaller Pt particles. This was derived from XPS measurements of the core-level binding energy of electrochemically aged Pt particles on a glassy carbon electrode. However, as pointed out already by Wertheim et al. as well as by Kuhrt et al.,[5,15] this apparent higher binding energy is caused by an artifact of the XPS, that is, the Coulomb energy of the charged final state.

* Author to whom correspondence should be addressed. E-mail: karl.mayrhofer@gmx.net.

† Present address: Physical Chemistry Department I, Technical University Munich.

10.1021/jp051735z CCC: $30.25
Published on Web 07/13/2005

Nevertheless, a similar conclusion was drawn from in-situ XAS studies by Mukerjee et al.,[16] namely, the adsorption of OH, among other molecules, is stronger on smaller particles and could inhibit the oxygen reduction reaction to a certain extent.

As in the case of the ORR, the relationship between the particle size and catalytic activity has also been discussed for the oxidation of CO on Pt supported on gold,[4,17] as well as on carbon.[18,19] However, contrary to what is expected from the particle-dependent Pt-oxygen energetics[14,16] and the proposed Langmuir−Hinshelwood reaction mechanism,[20] in a so-called CO-stripping experiment, a CO-monolayer is oxidized at a higher overpotential on smaller particles compared to larger ones or bulk polycrystalline Pt. This was initially accounted for by a change in reaction mechanism from the classically valid Langmuir−Hinshelwood (L−H) to Eley−Rideal, inferred from time-dependent transient measurements.[4] That this is very unlikely was shown recently by density functional calculations for CO monolayer oxidation on Pt clusters.[21] DFT calculations predicted that a full layer of CO inhibits the possibility of reaction with water molecules even at high overpotentials and that reaction can be initiated by dissociative adsorption of water at a vacancy adjacent to an adsorbed CO. Further insight into the particle size effect has been obtained from chronoamperometry, where the shape of CO stripping transient currents has been modeled employing the active site model.[22] The model for *perfect* cubooctahedral particles suggested restricted CO mobility (reduced activity) at Pt nanoparticles below ca. 2 nm size and a transition toward fast diffusion (enhanced activity) when the particle size exceeds 3 nm. Unfortunately, the model did include neither the competitive adsorption of anions in acid electrolyte (which can control the adsorption of OH[11] as well as the mobility of coadsorbed CO[23]) nor the existence of irregularities on nanoparticles, which, as for extended single-crystal surfaces, may serve as the active centers for OH adsorption.[24] Only recently it has been pointed out that Pt particles are unlikely to be perfect in the sense of having exactly the right number of atoms to form a regular body,[25] that is, a cubooctahedron in case of an fcc metal, and that the concentration of particularly low-coordinated surface atoms diverges well from the values of the actual perfect form. On the basis of this observation, it was proposed that the origins of the particle size effect for the oxidative removal of a preadsorbed monolayer of CO is the particle size dependent number of irregularities or defect sites.

In extension of the viewpoint that geometric and electronic effects are intimately entrenched, in this paper we will discuss the origins of the Pt particle size effect on electrosorption and catalytic processes. First, a method is introduced for establishing the potential of zero total charge (pztc) as a function of particle size. The values of pztc are used to develop a physical picture of the trends for adsorption of oxygenated species, hereafter denoted as OH, on the Pt clusters. Moreover, the impact of the electronically induced potential shift in the OH adsorption will be demonstrated at two electrochemical reactions, in which adsorbed OH is on one hand an educt species and promotes the reaction and on the other hand can act as a surface site blocking species and inhibits the reaction, namely, the CO bulk oxidation and the ORR.

2. Experimental

Catalyst Samples. Four different Pt high surface area catalysts were used in this study. Three samples, supplied by TKK (Tokyo, Japan), were carbon-supported Pt nanoparticles with mean diameters of 1−1.5 nm, 2−3 nm, and 5 nm, respectively (analysis by TKK). The fourth sample, consisting of a nanostructured Pt film supported on crystalline organic whiskers,[26] was supplied by 3M Company (St. Paul, MN). On the basis of the charge required to form a full monolayer of adsorbed hydrogen (the so-called H_{upd} charge), on the latter sample a specific surface area of about 8 m^2/g could be established, which would be equivalent to a cubooctahedral particle of ca. 30 nm diameter. In the following, the catalysts will simply be denoted as 1, 2, 5, and 30 nm catalysts. The Pt loading of the catalyst was roughly 20% for the 1 nm and 2 nm catalysts and 50% and 91% for the 5 nm and 30 nm samples, respectively. All analyses of the samples are conducted under the reasonable assumption that the metal−support interaction is negligible.[25,27] HR-TEM images of all catalysts have been published in our previous work.[28]

Electrochemical Measurements. The electrochemical measurements were conducted in a thermostated standard three-compartment electrochemical cell, using a ring-disk electrode setup with a bipotentiostat and rotation control (Pine). A saturated Calomel electrode (SCE), separated by an electrolytic bridge from the main cell compartment, was used for every experiment, however, all potentials are given with respect to the reversible hydrogen electrode (RHE). To minimize the error from the potential reading especially for the ORR, the hydrogen oxidation/evolution reaction was measured shortly before or after the ORR at 333 K or the CO-bulk oxidation at 298 K to calibrate the RHE relative to the Calomel electrode. A Pt mesh was used as a counter electrode. The electrolyte was prepared using pyrolitically triply distilled water and concentrated $HClO_4$ (Aldrich).

The preparation procedure for the high surface area catalyst has been described previously.[28] In short, the catalyst was dispersed ultrasonically in ultrapure water to concentrations between 0.3 and 1 $mg_{catalyst}/mL$, and a volume of 20−40 μL of the suspension was pipetted onto a polished glassy carbon substrate (6-mm diameter, 0.283 cm^2 geometrical surface area) leading to a Pt loading of 14 $\mu g_{Pt}/cm^2$ for the carbon-supported catalysts (TKK 1, 2, and 5 nm) and 42 $\mu g_{Pt}/cm^2$ for the 3M (30 nm) sample. After the evaporation of the water in an argon stream, 20 μL of a diluted Nafion solution (5wt %, Fluka) was pipetted onto the glassy carbon to attach the catalyst particles to the substrate. The thus prepared electrode was then transferred to the electrochemical cell protected by a drop of ultrapure water and was emersed under potential control at 0.05 V in argon-saturated 0.1 M $HClO_4$ solution. The potential was then constantly cycled between 0.05 V and 1.0 V till a stable cyclovoltammogram was recorded. For the oxygen reduction reaction (ORR), the electrolyte was purged with oxygen (Airgas), and the electrochemical cell was heated to 333 K. To avoid corrosion of the support or the catalyst itself, the positive limit of 1.0 V was never exceeded in any experiment. For the CO-bulk oxidation, the electrolyte was purged with CO at a constant electrode potential of 0.05 V for 15 min. After full saturation, the potential was cycled four times between 0.05 and 1.0 V with 20 mV/s, 1600 rpm, and constant CO-supply to CO-anneal the surface and achieve reproducible results.[25] The stable fifth sweep was recorded with 1 mV/s and 1600 rpm in the same potential region. After the reactions of interest were studied, a cyclovoltammogram was recorded at 298 K and was compared to the initial one to analyze eventual changes of the surface. Additionally, the CO-stripping behavior of every catalyst was studied in CO-free Ar purged solution, after adsorbing CO at a potential of 0.05 V until the electrode was completely covered. The active surface area was estimated using

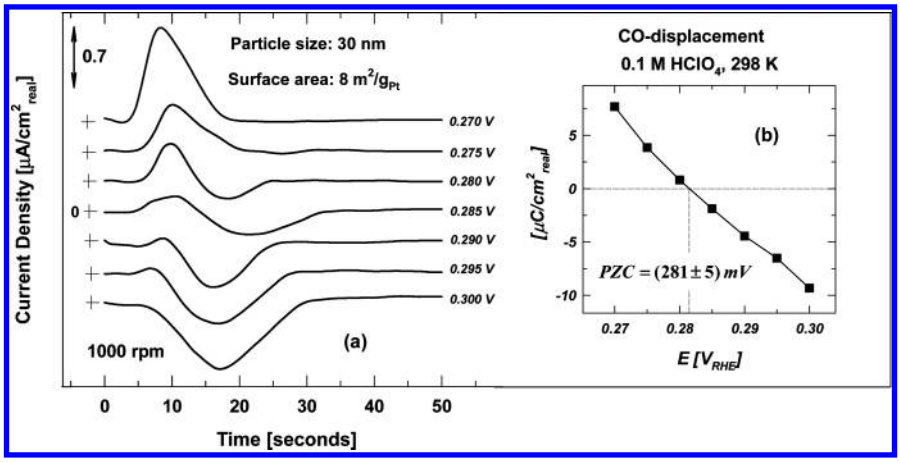

Figure 1. CO-displacement method for determining the pztc of carbon-supported high surface area catalysts, exemplified for the 30 nm catalyst. Displacement charge versus time after introducing CO into the system (a), measured in 0.1 M $HClO_4$ at 298 K with a rotation rate of 1000 rpm. The individual curves are offset from zero for clarity. Inset (b): Integrated charge under the CO-displacement peak versus the applied potential. The pztc corresponds to the potential where the regression crosses zero.

the peak area under the CO-stripping peak according to ref 29. For the measurement of the pztc, the CO-displacement method recently described by Climent et al.[30] was employed. CO was introduced into the Ar-purged electrolyte at a constant potential, and the resulting displacement current was recorded with time.

3. Results and Discussion

3.1. The Potential of Zero Charge (pzc). Frumkin and Petrii[31] first introduced the fundamental definitions describing the important impact of adsorption processes at the metal−electrolyte interface on the pzc, that is, the potential of zero free charge (pzfc) and the potential of zero total charge (pztc). A direct relationship exists between the pzfc of an electrode, the point where the truly free, electronic excess charge density on the metal surface equals zero, and its work function in UHV.[8,32] However, specific adsorption in electrolyte solution alters this potential, so that the only experimentally accessible parameter is the pztc, the point at which the free, electronic excess charge density plus the charge density transferred during adsorption processes equals zero. Only in the absence of specific adsorption, that is, on ideally polarizable electrodes, should these two potentials coincide, which is, however, not the case for Pt-electrodes. As a consequence, the measured pztc's are not absolute values for electrode surfaces and cannot be compared between different electrolytes. When acquired under the same conditions, however, perception of the changes in surface properties of various Pt-electrodes can be gained.

Among the experimental strategies used for estimating the pztc of Pt-electrodes, the recently described CO-displacement method by Climent and co-workers[30] is probably the most elegant one. In a potential region up to about 0.5 V, CO is strongly and irreversibly adsorbed on Pt; consequently, at a certain electrode potential, CO displaces the generally weaker adsorbed anions and cations completely. Moreover, no net charge is considered to pass through the interface during the adsorption of CO on the surface, thus the resulting transient charge depends solely on the relative amount of initially adsorbed species. Assuming that the charge density remaining on the metal surface can be neglected and no other reactions occur,[32,33] the pztc corresponds to the potential at which a charge density curve plotted against displacement potential crosses zero. Minimizing the effort, it was sufficient for extended Pt surfaces to obtain the displaced charge only at one single potential and refer the integrated voltammetric profile to this value.[30] For a high surface area catalyst, however, the overwhelming capacity of the carbon support would tamper thus received results. Hence, the CO-displacement charge was obtained at several potentials individually, as shown exemplarily for the 30 nm catalyst in Figure 1.

On the left-hand side, the measured current density is displayed versus time, with the introduction of CO into electrolyte being at $t = 0$. The curves are offset relative from zero so that they can easily be distinguished from each other. No current is noticed in the delay period that it takes CO to diffuse to the electrode surface. Moreover, after the displacement took place and the surface is completely covered by CO, the current drops to zero again. At potentials negative of the pztc, the measured displacement charge is positive, which means that the initially present adsorbate was mainly cations (predominantly adsorbed hydrogen, which hereafter will be defined as H_{upd}[20]). Coming closer to the pztc, negative parts appear in the displacement curve, and at even higher potentials, the latter takes over, indicating that adsorbed anions (OH^-, ClO_4^-) are displaced by CO. Using a straight line between the initial delay and the end status for background subtraction, the charge density can be calculated and plotted versus the displacement potential (insert Figure 1b). As already mentioned, the potential at which this curve crosses zero is considered as the pztc of the electrode in this electrolyte. For the 30 nm catalyst, a pztc of about 0.28 V was found; an average error of roughly ±5 mV is expected from the analysis of the three sets of independent measurements for all the high surface area catalysts. The results for the other three catalysts are summarized in Figure 2, where they are plotted against the inverse of the particle size. The pztc drops linearly from approximately 0.28 V for the 30 nm particles to 0.245 V for the 1 nm catalyst. This trend is in accordance with studies on stepped Pt single-crystal surfaces, where increasing the step density leads to a decrease in the pztc, although the effect is slightly greater on latter samples.[34,35] A polycrystalline Pt sample exhibited a pztc of ∼0.285 V (not shown) under the same conditions, which backs our assumption that the Pt support interaction is negligible. Interestingly, the ratio of surface atoms to the total amount of atoms, that is, the dispersion of the catalyst, as described by the average coordination number for ideal cubooctahedrons[6] in Figure 2 is also linear, confirming that the electronic (pztc) and geometric (average coordination number) factors are closely related.

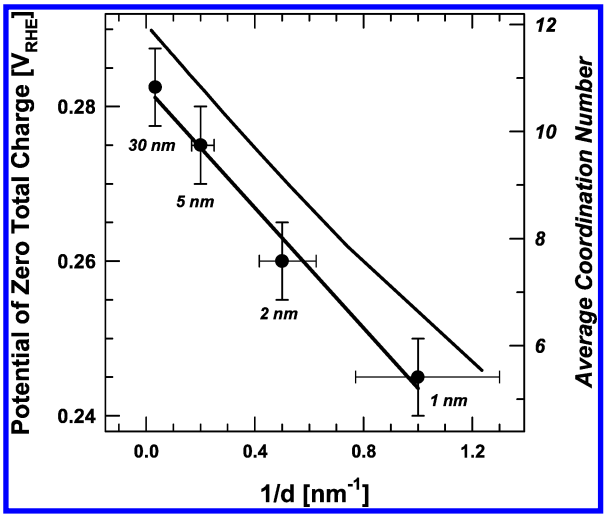

Figure 2. Variation of the potential of zero total charge with 1/*d*. The error of the displacement method is approximately 5 mV. The average coordination number of atoms in ideal cubooctahedral particles, taken from a model by Montejano et al.,[6] is plotted against the same *x*-scale.

On the basis of this observation, it appears that the *surface* electronic properties of each nanoparticle are unique, although the *bulk* electronic properties, given by the Fermi level of the material (the chemical potential μ), do not change decisively in this nanometer range. This effect can be understood in terms of the extent of electron "overspill" as a function of surface geometry.[36] The greater the overspill, that is, the more atoms per unit surface area or the lower the dispersion, the larger will be the surface dipole (the surface potential μ_e^M) and thus the work function ($\Phi^M N_A = \mu_e^M + F\chi^M$). As discussed by Trasatti,[8] the change in the work function can be directly correlated to the changes in the potential of zero total charge at the metal−solution interface. The variations in the pztc, in turn, will affect the electrosorption properties of the metal catalyst.[37] In line with Frumkin's and Trasatti's approach, Plieth[38] described the correlation between the shift in the likewise surface-specific redox potential of metal clusters in a dispersed state and other electrochemical properties including the pzc in a simple phenomenological model using first-order calculations. He suggested that a cathodic shift of the equilibrium oxidation potential is indirectly proportional to the particle diameter *d*, which goes hand in hand with a negative shift of the potential of zero charge and a decrease in the work function of the electrode surface by

$$\Delta\epsilon_D = \epsilon_d - \epsilon_b = -\frac{4\gamma v_M}{zF}\frac{1}{d} \qquad (1)$$

$\Delta\epsilon_D$ is thus the difference in equilibrium oxidation potentials between the dispersed ϵ_d and the bulk metal ϵ_b, v_M is the molar volume, and γ is the surface tension, which is considered constant in a first-order approximation (F is the Faraday constant, and z is the number of electrons transferred upon the metal oxidation). The surface tension is usually referred to vacuum and will most likely not be directly applicable in electrolyte, depending on the double-layer properties.

In agreement with eq 1, in our experiments, we observed a relatively small, yet clearly discernible, negative shift in the pztc of ca. 35 mV difference between the 30 and 1 nm Pt nanoparticles, when the average coordination number drops in parallel from about 11.7 to 6. Electrosorption properties, such as the formation of H_{upd} or the adsorption of anions from the supporting electrolyte, will be strongly particle size dependent

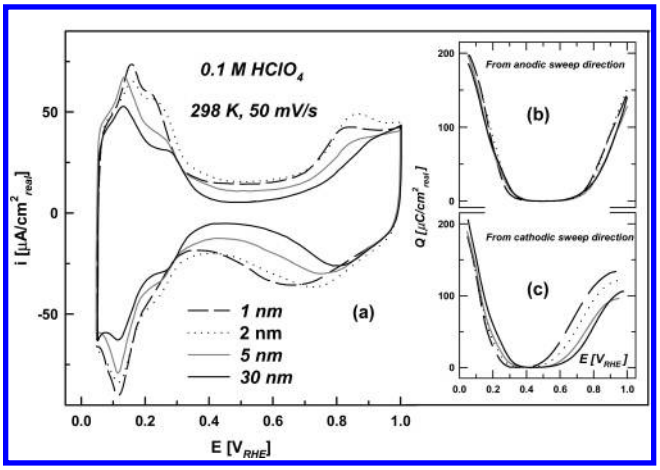

Figure 3. Cyclovoltammograms of the catalysts recorded in perchloric acid at room temperature with 50 mV/s (a). The insets depict the background-corrected, integrated charge density against the potential for the anodic (b) and the cathodic sweep direction (c), respectively.

because of this shift in the pztc, which will be further examined with particular focus on the adsorption of OH.

3.2. The Influence of the Particle Size on the Adsorption of Oxygenated Species. Although the features in the cyclovoltammograms of high surface area catalysts have been described previously in the literature, for example, refs 25 and 39, the results for the catalysts utilized in our measurements will be briefly discussed to complement and support the presented work. In Figure 3, CVs for the catalysts with a particle size of 1, 2, 5, and 30 nm, respectively, and the according adsorption/desorption isotherms are presented. Since a comparison of the original voltammograms is not quite as straightforward as for single crystals[20] because of the changing surface area of the respective catalysts, the current signal as well as the integrated charge was normalized in terms of the specific surface area (cm^2_{real}) using the charge under the H_{upd}−area, as described in ref 29. Furthermore, the isotherms in Figure 3b and c were calculated from the CV's by applying a background correction for the varying double-layer capacitance, which is mainly due to the different Pt-loadings of the catalysts and the resulting support contributions.

The three characteristic potential regions for Pt electrodes are well defined in Figure 3a for all voltammograms: the so-called H_{upd}-region between 0.05 V and 0.35 V is followed by the double-layer potential region up to about 0.7 V, where in turn the adsorption of oxygenated species begins. The peaks in the H_{upd}-region are generally not as distinct as for polycrystalline Pt,[20] especially the one at about 0.25 V seems to become less pronounced or to merge slightly toward more negative potentials relatively with decreasing particle size. This is also observable in the isotherms on the right-hand side, in particular, on the cathodic sweep where the relatively high sweep rate of 50 mV/s positively distorts the effect. When taking an average of both isotherms (not shown) to get rid of the sweep rate impact, the negative shift of the H_{upd}-region with decreasing particle size is still distinct, ca. 25 mV from 30 nm to 1 nm particles. Notice that the onset of hydrogen adsorption on Pt is not only determined by the Pt−H energetics itself but in addition by the Pt−anion interaction.[20] The negative shift of the H_{upd}-region with decreasing particle size can therefore also be associated with an enhanced anion adsorption due to the changes in the electronic surface properties. The impact of the pztc becomes even more obvious for the adsorption and desorption of oxygenated species at more positive potentials. Although apparently explicit from the actual voltammograms at first

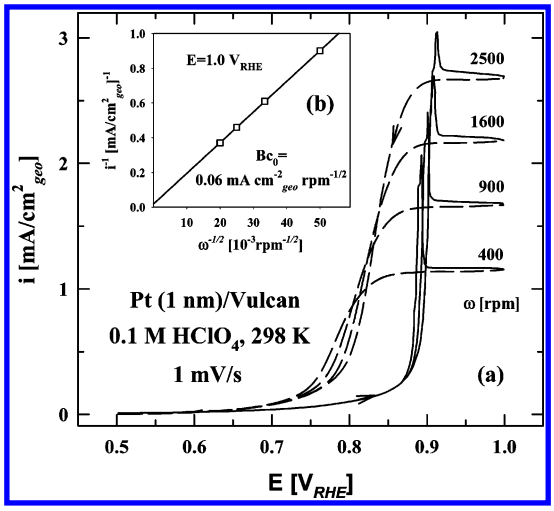

Figure 4. CO-bulk oxidation on the CO annealed 1 nm catalyst at rotation rates of 400, 900, 1600, and 2500 rpm (a). The measurements were conducted in 0.1 M perchloric acid at 298 K, with a sweep rate of 1 mV/s. The according Levich−Koutecky plot for a potential in the diffusion-limited region is displayed in b.

glance, somehow the negative shift of the adsorption of OH with decreasing particle size is not so demonstrative for the anodic sweep in the isotherms after double-layer capacity correction. However, the maximum of the oxide reduction peak in the cathodic sweep is shifted by more than 130 mV toward negative potentials for 1 nm particles compared to 30 nm particles, with the 2 nm and 5 nm particles lying in-between. This is also clearly reflected in the isotherm in Figure 3c, confirming that smaller particles are more irreversible oxidized at lower potentials than larger ones, that is, the oxophilicity of particles increases with decreasing particle size.

A stronger adsorption of oxygen atoms on smaller particles is also well documented in the gas phase,[40] where it has been found that oxygen atoms appear to dissolve quite easily into small metal particles, so that a clear distinction between chemisorption and bulk oxidation cannot always be drawn. As a consequence, in heterogeneous catalysis, the decrease in the rate of oxidation reaction of organic molecules with decreasing the particle size is usually attributed to a stronger adsorption of oxygen atoms on smaller particles. Along the same line, in electrocatalysis, the variation in the affinity for the oxygen species with the particle size will control the catalytic activity of the Pt nanoparticles. So by focusing on the potential region where the adsorption/desorption of oxygenated species occurs, we will now investigate how these changes in the oxophilicity can affect in particular the CO bulk oxidation and the ORR.

3.3. Oxygenated Species as Reaction Promoter: The CO-Bulk Oxidation. As pointed out in the Introduction, the CO-stripping method has been used preferably to establish the particle size effects in the CO oxidation reaction.[4,19,25] The thus observed increasing activities with increasing particle size are in contradiction to what is expected considering the trend in the pztc as discussed in the previous section. To correlate the catalytic activity of nanoparticles with the oxophilicity, however, it was suggested that the kinetic activity for the CO oxidation reaction should rather be studied via the CO bulk method,[28] that is, in a CO saturated solution and under the well-defined mass transport of CO molecules to the electrode surface.[41]

In Figure 4, the CO bulk oxidation is presented exemplarily on 1 nm particles for various rotation rates. No significant current was detected in the so-called preignition potential region up to about 0.8 V because of the pretreatment of the catalyst by CO-annealing.[25] At the ignition potential around 0.9 V, the CO oxidation currents increase sharply in a very narrow potential range, reaching a maximum and then declining back to the diffusion limited values. This unusual shape of the polarization curves at $E > 0.9$ V is determined by the superposition of two processes, the oxidation of the preadsorbed CO monolayer and the continuous oxidation of CO from the bulk solution. Notice in addition that the stripping peak on top of the diffusion-limited current is shorter but wider for higher rotation rates of the disk electrode and that the peak position is shifted slightly toward higher potentials, from 0.89 V for 400 rpm to 0.91 V for 2500 rpm. This can be attributed to the increased supply of CO toward the electrode[42] with the elevated rotation rate, which in turn can block the formation of the active OH adsorbants. The same effect can be seen on the negative going sweep at ca. 0.8 V, where the deactivation of the CO oxidation rate is the most pronounced for 2500 rpm. As shown in Figure 4, at 400 rpm, the kinetic region is extended to the most negative potentials because of the lesser diffusion of CO from the bulk.

Between 0.9 and 1.0 V, the CO bulk oxidation proceeds at the diffusion-limited rate. The magnitude of the diffusion-limited current is similar to the one obtained on extended surfaces,[43] so that the diffusion resistance of the Nafion film for the applied thin-film method is negligible for this reaction. This is also confirmed by the Levich−Koutecky plot in Figure 4b, where all data points lie on a straight line that intercepts at 54 mA/cm^2 and has a slope of 0.057 mAcm$^{-2}{}_{\mathrm{geo}}$rpm$^{-1/2}$. On the reversal of the sweep direction at 1.0 V, the electrode surface is predominantly covered by oxygenated species and therefore the kinetic region extends much further to negative potentials compared to the positive sweep. Depending on the rotation rate, and thereby on the supply of CO, the current signal starts to drop between 0.8 and 0.85 V and reaches zero at about 0.65 to 0.7 V. At this point, all adsorbed OH has been consumed by the reaction, and the whole electrode surface is again covered by a layer of CO, completely inhibiting the adsorption of reactive OH and thereby the CO oxidation.

If we focus on the specific activities that are obtained under the conditions where the surface is predominantly covered by oxygenated species (the negative sweep direction), then it is possible to study how the particle size dependent surface coverage by OH affects the kinetics of the CO bulk oxidation. This is shown in Figure 5 for the 1, 5, and 30 nm catalyst; for clarity reasons, the 2 nm particles, which exactly follow the demonstrated trend in activity, were left out. It can be clearly seen from the polarization curves that the kinetic region for the CO oxidation is extended to more negative potentials for smaller particles, with 30 nm revealing almost reversible behavior and becoming inactive already at the ignition potential in contrast to 1 nm, which is fairly active till about 0.8−0.82 V. This can also be retrieved from the Tafel-plot in the insert of Figure 5b, where the potential is plotted against the logarithmic current density, normalized to the specific surface area of the respective catalyst. Except for the 1 nm particles (∼33 mV/dec), no completely linear Tafel relationship could be detected for the CO oxidation in the cathodic sweep over more than 1 order of magnitude. The reason for this could be that the defect sites, which govern the reaction on CO precovered surfaces,[25] still have an impact in the reverse sweep to a certain degree. Nevertheless, the trend in the CO bulk activity can be unambiguously determined over the whole potential region of interest, which leads to a reaction order of 30 nm < 5 nm < 1 nm. Assuming that the L−H reaction mechanism for the CO oxidation reaction holds for carbon-supported Pt catalysts as it

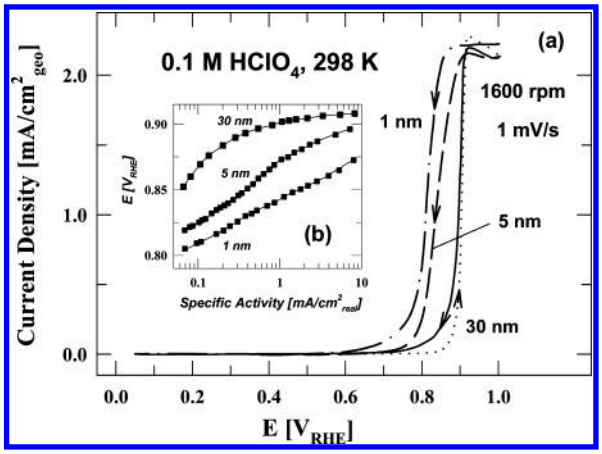

Figure 5. (a) Comparison of the CO bulk oxidation on the 1-, 5-, and 30 nm catalyst (the 2 nm catalyst is not shown for clarity) at the negative going sweep from 1.0 V where the surface is mainly covered with OH. Only the positive sweep of the 30 nm catalyst is illustrated for clarity, since the ignition potential is independent of the particle size. In the insert (b), the potential is depicted against the specific activity (Tafel plot).

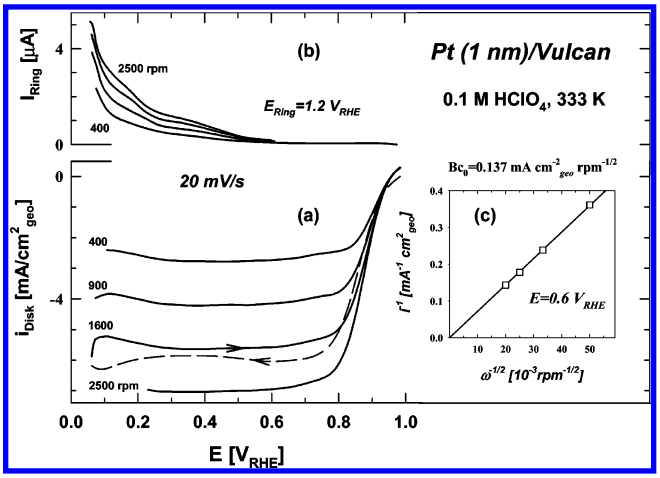

Figure 6. Polarization curves for the oxygen reduction reaction (a) and the peroxide production on the ring (b) exemplarily for the 1 nm catalyst at different rotation speeds. Experiments were conducted in 0.1 M perchloric acid at 333 K, with a scanrate of 20 mV/s. Insert c shows the Levich−Koutecky plot at 0.6 V (diffusion-limited region).

does for bulk Pt,[20] then this reactivity trend is in perfect agreement with the change in oxophilicity with the particle size as shown in section 3.2. Namely, the smallest particles, that is, 1 nm, with the most negative pztc adsorb OH at more negative potentials and as a consequence are more active for the CO oxidation. On the contrary, 30 nm particles with a more positive pztc are less oxophilic; therefore, the oxidation reaction is hindered to a higher degree.

3.4. Oxygenated Species as Reaction Inhibitor: The Oxygen Reduction Reaction. The ORR on Pt electrodes is well studied on bulk polycrystalline and single crystals as well as high surface area catalysts in various electrolytes.[44−46] Although effects such as the change in specific activity for oxygen reduction with the particle size have been reported previously[2,3,14,47] and confirmed several times, many important details related to the relationships between the rate of reaction and the size of Pt nanoparticles are still not completely resolved and remain puzzling. Therefore, we will focus below on the extent of the particle size effect at the analyzed catalysts and set it in relation to the other effects reported in the previous sections. In Figure 6, the ORR polarization curves are exemplarily depicted for the 1 nm catalyst at various rotation rates, supplementary also the produced peroxide has been detected at the ring.

As shown in Figure 6a, after sweeping the potential positive from 0.05 V, the diffusion-limiting currents are observed up to about 0.8 V. At more positive potentials, the ORR is first under diffusion-kinetic limitations and finally, for $E > 0.9$ V, under a pure kinetic control. In the cathodic sweep, which is only shown for 1600 rpm, a similar behavior can be found. However, a slight hysteresis in the kinetic region due to the irreversible adsorption of oxides at the electrode surface,[20] as well as a deviation due to the capacity of the high surface area catalyst, which can be clearly seen in the diffusion-limited region especially for the 1 nm catalyst at a sweep rate of 20 mV/s, exists on sweep reversal. The latter can be simply corrected for by subtracting the cyclovoltammogram recorded in Ar purged solution at the same sweep rate. Similar to the CO oxidation reaction, the Levich−Koutecky plot assessed from data at 0.6 V is shown in Figure 6c. Close to what has been reported in the literature for ORR on Pt electrodes,[20,48] the slope of the straight line, which intercepts at almost zero, has a slope of 0.137 $mAcm^{-2}_{geo}$ $rpm^{-1/2}$.

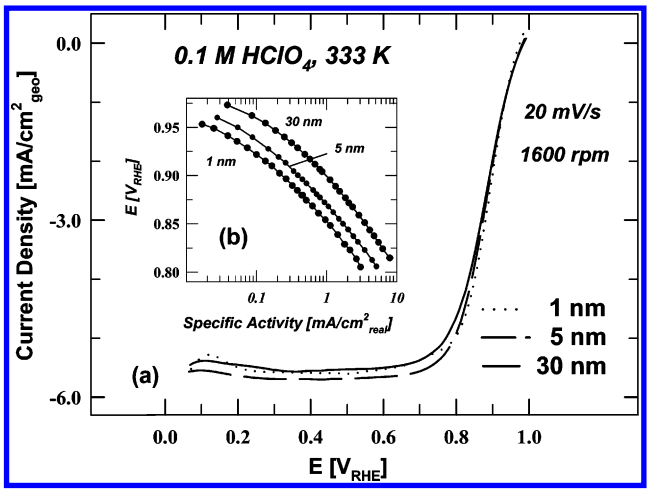

Figure 7. (a) Comparison of the oxygen reduction reaction on the 1, 5, and 30 nm catalyst (the 2 nm catalyst is not shown for clarity) at the positive going sweep. Only the cathodic sweep of the 30 nm catalyst is illustrated. In the insert (b), the potential is depicted against the specific activity (Tafel plot).

Interestingly, the kinetic region of the ORR spreads over the same potentials where also the kinetics of the CO oxidation changes dramatically. Contrary to what we have seen for the CO bulk oxidation, however, adsorbed OH is not a necessary reactant but rather a product of the reaction.[49] Notice that OH_{ad} can also be formed in acid electrolyte by the dissociation of water at the electrode surface (section 3.2). In either case, the adsorbed OH is considered to be a spectator species and thus reduces the number of active sites for the ORR to proceed.[20] Considering that the surface coverage by OH is particle size dependent, one may expect that the kinetics of the ORR will also be determined by the oxophilicity of Pt nanoparticles.

The anodic polarization curves given in Figure 7a for 1, 5, and 30 nm catalysts at 1600 rpm exhibit the same diffusion-limited current and are overlapping in the kinetic region. To obtain meaningful, comparable data, they have to be corrected for the specific surface area, which was determined from CO stripping experiments.[29] The results are depicted in the logarithmic Tafel plot in the insert of Figure 7b for the kinetic region between 0.95 and 0.85 V. A clear trend can be seen for the activity of the oxygen reduction over the whole potential range, that is, the smaller the particles the lower the specific current

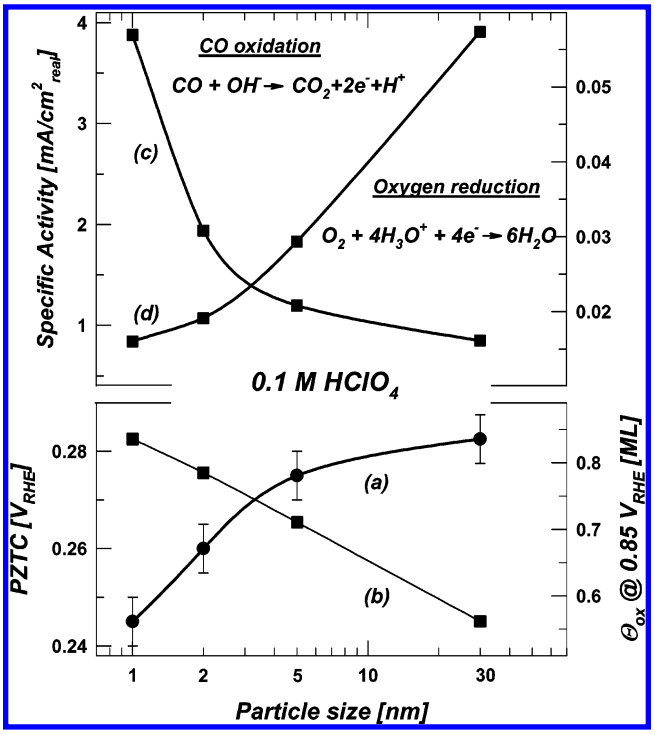

Figure 8. Summary of the results from the CO-displacement (a) and cyclovoltammetry (b), as well as from CO bulk oxidation (c) and oxygen reduction reaction (d), showcasing the adsorption of OH and its impact on the electrochemistry at the Pt electrode−solution interface depending on the particle size.

density. Unfortunately, it was not possible to fit one single linear approximation into the plots and determine the Tafel slope because of the continuous increase of the slope with increasing potential. When comparing different particles, however, the shape of the curves only changes negligibly, which indicates that the same reaction mechanism is most likely valid for all catalysts. Furthermore, it appears that the Tafel plots for different particle sizes are shifted parallel to each other, from 1 nm to 30 nm for about 50 mV or by a factor of 6 when expressed on a potential scale or as specific current density, respectively. This is in excellent agreement with the shift in the pztc of approximately 35 mV and the concomitant trend in oxophilicity as described in section 3.1 and 3.2.

4. Summary and Conclusion

The crucial particle size dependent adsorption of oxygenated species at the Pt surface in acid electrolyte was discussed with regard to the variation in the physical−chemical characteristics of nanoparticles. Additionally, the impact on two important practical electrochemical reactions was demonstrated as support of our considerations, which are summarized in Figure 8 and in the main conclusions below.

The potential of total zero charge shifts approximately 35 mV negative by decreasing the particle size from 30 nm down to 1 nm (Figure 8a). In agreement with Frumkin and Petrii,[37] we found that the electrosorption properties of the metal catalysts are therefore also dependent on the cluster size. The Pt−H_{upd} interactions appear to be weaker on smaller particles, whereas the energy of adsorption of anions, in particular OH, is more enhanced, that is, at the same potential the surface coverage by oxygenated species increases by decreasing the particle size (Figure 8b).

The reaction kinetics of the CO bulk oxidation (Figure 8c) as well as of the ORR (Figure 8d) are dependent on the particle size, in complete agreement with the variation of the oxophilicity, that is, the coverage with oxygenated species. If adsorbed OH is a promoter of a reaction as for the L−H CO bulk oxidation, then an increase in oxophilicity with a decrease in particle size results in increased specific activity. On the contrary, for the ORR the increase in oxophilicity with smaller particles leads to a decrease in specific activity, because OH can effectively block the active sites required for the adsorption of O_2 or the splitting of the O−O bond, in agreement with single-crystal work.[20] The parallel shift in the Tafel plots (Figure 7b) indicates that the same reaction mechanism is most likely valid for the different Pt catalysts. Furthermore, the kinetics are not determined by the Pt-oxygen energetics but rather by the adsorption isotherm of oxygenated spectator species, generated from the dissociation of water at the Pt-surface in acid electrolyte.

Our results clearly indicate that as in heterogeneous catalysis, at the electrified metal−solution interface, the catalytic activity is determined by the interplay of surface geometric and electronic factors. Since the distribution of surface atoms varies with the characteristic dimension of aggregates, which was described in our case by the dispersion of the catalyst (average coordination number), each size cluster exhibits unique electronic properties, as demonstrated in this work by the potential of zero total charge. This can be considered as the origin of the variation of the reaction rate with the particle size for the reactions presented here.

Acknowledgment. This work was supported by the Director, Office of Science, Office of Basic Energy Sciences, Division of Materials Sciences, U.S. Department of Energy under Contract No. DE-AC03-76SF00098. K.M. acknowledges his supervisor Prof. Christoph Fabjan at the TU Vienna and the Austrian BMBWK for a Ph.D. scholarship. Furthermore, we would like to thank Adams & Chittenden Scientific Glass for the electrochemical cells and T. Tomoyuki from TKK as well as R. Atanasoski and M.K. Debe from 3M for the supply with the catalyst samples.

References and Notes

(1) Boudart, M. *Adv. Catal.* **1969**, 153.
(2) Bregoli, L. J. *Electrochim. Acta* **1978**, *23*, 489−492.
(3) Sattler, M. L.; Ross, P. N. *Ultramicroscopy* **1986**, *20*, 21−28.
(4) Friedrich, K. A.; Henglein, F.; Stimming, U.; Unkauf, W. *Colloids Surfs., A* **1998**, *134*, 193−206.
(5) Kuhrt, C.; Harsdorff, M. *Surf. Sci.* **1991**, *245*, 173−179.
(6) Montejano-Carrizales, J. M.; Aguilera-Granja, F.; Moran-Lopez, J. L. *Nanostruct. Mater.* **1997**, *8*, 269−287.
(7) Henry, C. R. *Surf. Sci. Rep.* **1998**, *31*, 231−325.
(8) Trasatti S. *Advances in Electrochemistry and Electrochemical Engineering*; Wiley: New York, 1977; p 221.
(9) Trasatti, S.; Parsons, R. *J. Electroanal. Chem.* **1986**, *205*, 359−376.
(10) Kinoshita, K. *Electrochemical Oxygen Technology*; Wiley and Sons: New York, 1990.
(11) Markovic, N. M.; Radmilovic, V.; Ross, P. N. *Catalysis and Electrocatalysis at Nanoparticle Surfaces*; Marcel Dekker: New York, 2003.
(12) Watanabe, M.; Sei, H.; Stonehart, P. *J. Electroanal. Chem.* **1989**, *261*, 375−387.
(13) Giordano, N.; Passalacqua, E.; Pino, L.; Arico, A. S.; Antonucci, V.; Vivaldi, M.; Kinoshita, K. *Electrochim. Acta* **1991**, *36*, 1979−1984.
(14) Takasu, Y.; Ohashi, N.; Zhang, X.-G.; Murakami, Y.; Minagawa, H.; Sato, S.; Yahikozawa, K. *Electrochim. Acta* **1996**, *41*, 2595−2600.
(15) Wertheim, G. K.; DiCenzo, S. B.; Buchanan, D. N. E. *Phys. Rev. B* **1986**, *33*, 5384.
(16) Mukerjee, S.; McBreen, J. *J. Electroanal. Chem.* **1998**, *448*, 163−171.
(17) Friedrich, K. A.; Henglein, F.; Stimming, U.; Unkauf, W. *Electrochim. Acta* **2000**, *45*, 3283−3293.
(18) Cherstiouk, O. V.; Simonov, P. A.; Savinova, E. R. *Electrochim. Acta* **2003**, *48*, 3851−3860.

(19) Cherstiouk, O. V.; Simonov, P. A.; Zaikovskii, V. I.; Savinova, E. R. *J. Electroanal. Chem.* **2003**, *554*−*555*, 241−251.
(20) Markovic, N. M.; Ross, J. *Surf. Sci. Rep.* **2002**, *45*, 117−229.
(21) Dunietz, B. D.; Markovic, N. M.; Ross, P. N.; Head-Gordon, M. *J. Phys. Chem. B* **2004**, *108*, 9888−9892.
(22) Maillard, F.; Eikerling, M.; Cherstiouk, O. V.; Schreier, S.; Savinova, E.; Stimming, U. *Faraday Discuss.* **2004**, *125*, 357−377.
(23) Stamenkovic, V. R.; Chou, K. C.; Somorjai, G. A.; Ross, P. N.; Markovic, N. M. *J. Phys. Chem. B* **2005**, *109*, 678−680.
(24) Lebedeva, N. P.; Koper, M. T. M.; Feliu, J. M.; van Santen, R. A. *J. Phys. Chem. B* **2002**, *106*, 12938−12947.
(25) Arenz, M.; Mayrhofer, K. J. J.; Stamenkovic, V. R.; Blizanac, B. B.; Tada, T.; Markovic, N. M.; Ross, P. N. *J. Am. Chem. Soc.* **2005**, *127*, 6819−6829.
(26) Debe, M. K. *Handbook of Fuel Cells - Fundamentals, Technology and Applications*; John Wiley & Sons: New York, 2002; pp 576−589.
(27) Arico, A. S.; Antonucci, V.; Antonucci, P. L. *Catalysis and Electrocatalysis on Nanoparticle Surfaces*; Marcel Dekker: New York, 2003; Chapter 17, p 613.
(28) Mayrhofer, K. J. J.; Arenz, M.; Blizanac, B. B.; Stamenkovic, V. R.; Markovic, N. M.; Ross, P. N. *Electrochim. Acta* **2005**, submitted.
(29) Kinoshita, K.; Stonehart, P. *Modern Aspects of Electrochemistry*; Plenum Press: New York, 1977; Chapter 4, p 183.
(30) Climent, V.; Gomez, R.; Orts, J. M.; Rodes, A.; Aldaz, A.; Feliu, J. M. *Interfacial Electrochemistry*; Marcel Dekker: New York: 1999; p 463.
(31) Frumkin, A. N.; Petrii, O. A. *Electrochim. Acta* **1975**, *20*, 347−359.
(32) Weaver, M. J. *Langmuir* **1998**, *14*, 3932−3936.
(33) Cuesta, A. *Surf. Sci.* **2004**, *572*, 11−22.
(34) Climent, V.; Gomez, R.; Feliu, J. M. *Electrochim. Acta* **1999**, *45*, 629−637.
(35) Climent, V.; Attard, G. A.; Feliu, J. M. *J. Electroanal. Chem.* **2002**, *532*, 67−74.
(36) *Topics in Applied Physics - Photoemission in Solids I*; Springer-Verlag: Berlin, 1978.
(37) Frumkin, A. N.; Petrii, O. A.; Damaskin, B. B. *Comprehensive Treatise of Electrochemistry*; Plenum Press: New York, 1980; p 221.
(38) Plieth, W. J. *J. Phys. Chem.* **1982**, *86*, 3166−3170.
(39) Gasteiger, H. A.; Kocha, S. S.; Sompalli, B.; Wagner, F. T. *Appl. Catal., B* **2005**, *56*, 9−35.
(40) Fuentes, S.; Figueras, F. *J. Chem. Soc., Faraday Trans.* **1978**, *74*, 174.
(41) Albery, W. J.; Hitchman, M. L. *Ring Disk Electrodes*; Claredon Press: Oxford, U.K., 1971.
(42) Markovic, N. M.; Schmidt, T. J.; Grgur, B. N.; Gasteiger, H. A.; Behm, R. J.; Ross, P. N. *J. Phys. Chem. B* **1999**, *103*, 8568−8577.
(43) Markovic, N. M.; Grgur, B. N.; Lucas, C. A.; Ross, P. N. *J. Phys. Chem. B* **1999**, *103*, 487−495.
(44) Markovic, N. M.; Adzic, R. R.; Cahan, B. D.; Yeager, E. B. *J. Electroanal. Chem.* **1994**, *377*, 249−259.
(45) Markovic, N. M.; Gasteiger, H. A.; Ross, P. N. *J. Phys. Chem.* **1995**, *99*, 3411−3415.
(46) Perez, J.; Villullas, H. M.; Gonzalez, E. R. *J. Electroanal. Chem.* **1997**, *435*, 179−187.
(47) Kinoshita, K. *J. Electrochem. Soc.* **1990**, *137*, 845.
(48) Paulus, U. A.; Schmidt, T. J.; Gasteiger, H. A.; Behm, R. J. *J. Electroanal. Chem.* **2001**, *495*, 134−145.
(49) Norskov, J. K.; Rossmeisel, J.; Logadottir, A.; Lindqvist, L.; Kitchin, J. R.; Bligaard, T.; Jonsson, H. *J. Phys. Chem. B* **2004**, *108*, 17886−17892.